

Shape Transitions of Domains in Insoluble Monolayers: Derivation and Use of Computationally Efficient Formulations of the Electrostatic Energy

M. A. Mayer and T. K. Vanderlick*

Department of Chemical Engineering, University of Pennsylvania,
Philadelphia, Pennsylvania 19104-6393

Received April 30, 1992. In Final Form: September 23, 1992

Dispersed domains in a two-phase insoluble phospholipid monolayer exhibit a myriad of shapes. Domain shapes can be predicted using a free energy analysis put forth by McConnell. One contribution to the free energy of an isolated domain is the electrostatic energy arising from dipolar interactions between lipid molecules. The expression for this electrostatic energy, however, cannot be evaluated analytically and is cumbersome to compute numerically. In this paper, we derive two simplified, yet rigorous, formulations of the electrostatic energy, one being more computationally efficient for circular domains, the other for noncircular domains. We used these rigorous expressions to repeat two previously reported shape calculations that were based on an approximation to the electrostatic energy. Our results differ from the original results by an amount proportional to the domain perimeter, offering a bridge between our energy functional and the approximated one.

1. Introduction

Monomolecular films of phospholipids residing at the air-water interface undergo a variety of two-dimensional phase transitions. In one particular two-phase regime, a so-called liquid-condensed phase coexists with a less dense liquid-expanded phase. The liquid-condensed phase is dispersed in the form of domains which can be directly visualized using the technique of fluorescence video microscopy.¹⁻⁶ A myriad of different domain shapes have been experimentally observed. While different lipid monolayers each form domains of a characteristic shape, a given monolayer may exhibit reversible shape transitions when, for example, the temperature or domain size is varied.⁷

Following the analysis of McConnell,⁸ the shape of an isolated domain results from a competition between line tension and electrostatic repulsion. The line tension arises from the excess free energy associated with the formation of the interface between the liquid-condensed domain and the surrounding liquid-expanded phase. This line tension acts to minimize the perimeter of a domain, thus promoting compact, circular shapes. The electrostatic energy arises from interactions between the oriented dipole moments of lipids anchored at the surface of water. The excess dipole density of the liquid-condensed phase relative to the liquid-expanded phase acts to form noncompact, needle-like domains. The predicted domain shape is the one that minimizes the free energy as given by the sum of interfacial and electrostatic contributions:

$$F = F^I + F^E \quad (1.1)$$

The interfacial free energy may be expressed as

$$F^I = \lambda P \quad (1.2)$$

where λ is the line tension and P is the perimeter of the

domain. If the domain is considered to be a collection of vertically oriented dipoles, the electrostatic energy may be expressed as

$$F^E = \frac{\mu^2}{2} \int \int g(|\mathbf{r}^* - \mathbf{r}|) |\mathbf{r}^* - \mathbf{r}|^{-3} d^2\mathbf{r}^* d^2\mathbf{r} \quad (1.3)$$

where μ is the average excess dipole density and $g(r)$ is the pair distribution function.

Physically, the pair distribution function must be zero at small separations to account for the nonoverlap of molecules; it approaches unity at large separations, where the density distribution becomes uncorrelated. The simplest pair distribution function which meets these criteria is the Heavyside step function:

$$g(|\mathbf{r}^* - \mathbf{r}|) = \mathcal{H}(|\mathbf{r}^* - \mathbf{r}| - \delta) = \begin{cases} 1 & |\mathbf{r}^* - \mathbf{r}| \geq \delta \\ 0 & |\mathbf{r}^* - \mathbf{r}| < \delta \end{cases} \quad (1.4)$$

where δ is a parameter representing the distance of closest approach between molecules. Mathematically, it is essential that any model chosen for the pair distribution function be of a form suitable to render the integrand of F^E nonsingular. Clearly, the Heavyside step function accomplishes this. Its presence, however, prevents analytic evaluation of the electrostatic energy. Furthermore, numerical evaluation is cumbersome because the integral is fourth order with an integrand which changes rapidly in the neighborhood of the singularity.

To simplify the evaluation of the electrostatic energy, McConnell⁸ proposed an approximation to F^E based on the analogy between a domain of dipoles and a capacitor of finite size:

$$F^E \approx \frac{2\pi}{t} A\mu^2 - \frac{1}{2}\mu^2 \iint_{|\mathbf{x}-\mathbf{x}^*|>\delta} \frac{d\mathbf{X}\cdot d\mathbf{X}^*}{|\mathbf{X}-\mathbf{X}^*|} \quad (1.5)$$

Here t is the capacitor thickness and \mathbf{X} is a vector from the origin to a point on the perimeter of the domain. McConnell and co-workers have used this capacitor approximation in the prediction of the equilibrium radius of circular domains⁹ and the transition from circular to elliptical domains.⁸ Vanderlick and M6hwald¹⁰ used it in

* To whom correspondence should be addressed.

- (1) Tscharner, V.; McConnell, H. M. *Biophys. J.* 1981, 36, 409.
- (2) Seul, M.; McConnell, H. M. *J. Phys. E* 1985, 18, 193.
- (3) Gaub, H. E.; Moy, V. T.; McConnell, H. M. *J. Phys. Chem.* 1986, 90, 1721.
- (4) Knobler, C. M. *Adv. Chem. Phys.* 1991, 77, 397.
- (5) Seul, M. *Physica A* 1990, 168, 198.
- (6) Fl6rsheimer, M.; M6hwald, H. *Chem. Phys. Lipids* 1989, 49, 231.
- (7) Heckl, W. M.; M6hwald, H. *Ber. Bunsen-Ges. Phys. Chem.* 1986, 90, 1159.
- (8) Keller, D. J.; Korb, J. P.; McConnell, H. M. *J. Phys. Chem.* 1987, 91, 6417.

(9) McConnell, H. M.; Moy, V. T. *J. Phys. Chem.* 1988, 92, 4520.

(10) Vanderlick, T. K.; M6hwald, H. *J. Phys. Chem.* 1990, 94, 886.

their prediction of shape transitions of domains with regularly undulating boundaries.

More recently, McConnell et al.^{11,12} proposed an alternative pair distribution function of a mathematically judicious form which produces a continuous, yet simple, integrand in the expression of the electrostatic energy. This pair distribution function is given by

$$\tilde{g}(|\mathbf{r} - \mathbf{r}^*|) = \frac{|\mathbf{r} - \mathbf{r}^*|^3}{((|\mathbf{r} - \mathbf{r}^*|^2 + 4\delta^2)^{1/2})^3} \quad (1.6)$$

Henceforth, we use the tilde notation to distinguish functionals based on $\tilde{g}(r)$ from those based on the Heavyside step pair distribution function. The free energy functional, \tilde{F} , is therefore given by $\tilde{F}^T + \tilde{F}^E$ where

$$\tilde{F}^E = \frac{\mu^2}{2} \iint \frac{d^2\mathbf{r}^* d^2\mathbf{r}}{((|\mathbf{r}^* - \mathbf{r}|^2 + 4\delta^2)^{1/2})^3} \quad (1.7)$$

Here the parameter δ no longer serves as a limit of integration, but is still on the order of the nearest-neighbor separation between molecules. An advantage of using $\tilde{g}(r)$ is that if the radius of curvature along the entire domain boundary is much longer than δ , then \tilde{F}^E reduces to¹²

$$\tilde{F}^E = \frac{\pi A}{\delta} \mu^2 - \frac{1}{2} \mu^2 \oint \oint \frac{d\mathbf{X} \cdot d\mathbf{X}^*}{(|\mathbf{X} - \mathbf{X}^*|^2 + 4\delta^2)^{1/2}} - P\mu^2 \quad (1.8)$$

where P denotes the perimeter. It can also be shown¹¹ that the integral term of the capacitor approximation, eq 1.5, equals the integral term in this expression for \tilde{F}^E . It follows, therefore, that if the line tension used in the capacitor approximation is artificially decreased by μ^2 , i.e., $\lambda_{CA} = \lambda - \mu^2$, the capacitor approximation is identical to \tilde{F}^E (except for the term which is proportional to the area).

It is not necessary, however, to reject the original (Heavyside) pair distribution function because of the complications associated with having a discontinuous integrand in the expression of the electrostatic energy: these can be overcome. In this paper, we develop two simplified, yet rigorous, formulations of this electrostatic energy. (Henceforth, the electrostatic energy based on the Heavyside function will be referred to as simply "the" electrostatic energy functional, and denoted by F^E). In the first formulation, Green's theorem is used to reduce both of the area integrals in eq 1.3 to contour integrals. The resulting expression allows us to identify explicitly the source of the difference between the capacitor approximation and the electrostatic energy functional. In the second formulation, a prudent coordinate transformation is used to reduce the integral in eq 1.3 from fourth to third order. This second expression can be computed more efficiently than the first, except in the case of circular or nearly circular domains. Finally, we describe quantitatively how results of certain domain morphology calculations (those based on circular domain shape) obtained using the capacitor approximation relate to the results based on the electrostatic energy functional.

2. Derivation of Two Simplified Electrostatic Energy Expressions

A. Reduction of the Area Integrals through Green's Theorem. In the first simplification of the electrostatic energy, both of the area integrals in eq 1.3 are reduced to contour integrals using Green's theorem:¹³

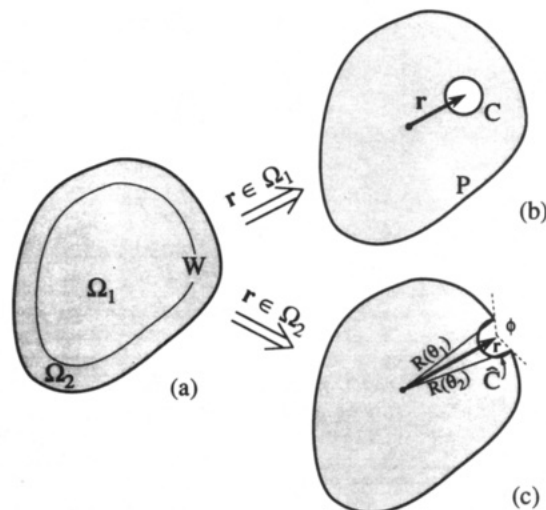


Figure 1. (a) Second application of Green's theorem which requires defining two distinct regions of the domain: Ω_1 is that portion of the domain further than δ from the perimeter, and Ω_2 is the remainder. The curve W separates Ω_1 and Ω_2 . (b) When $\mathbf{r} \in \Omega_1$, the boundary of Ω^* consists of two closed curves: the perimeter, P , and a circle of radius δ centered at \mathbf{r} , C . (c) When $\mathbf{r} \in \Omega_2$, the boundary of Ω^* is a single closed curve consisting of two parts: \hat{P} , the portion of P which is external to C , and \hat{C} , the portion of C which lies internal to Ω . \hat{C} intersects \hat{P} at the two angles θ_1 and θ_2 .

$$\int_D \nabla \cdot \mathcal{G} d^2\mathbf{r} = \oint_{\mathcal{C}} \mathbf{n} \cdot \mathcal{G} ds \quad (2.1)$$

where \mathcal{C} is the boundary of region \mathcal{D} and \mathbf{n} is the outward unit normal to \mathcal{C} . To do so, however, the electrostatic energy is first rewritten as

$$\frac{-F^E}{\mu^2/2} = - \iint \mathcal{H}(|\mathbf{r}^* - \mathbf{r}| - \delta) |\mathbf{r}^* - \mathbf{r}|^{-3} d^2\mathbf{r}^* d^2\mathbf{r} = \int_{\Omega} \int_{\Omega^*} \nabla^* \cdot \nabla \cdot \tau d^2\mathbf{r}^* d^2\mathbf{r} \quad (2.2)$$

Here Ω is all points of the domain, Ω^* , which is a function of \mathbf{r} , is that portion of Ω which meets the separation restriction $|\mathbf{r}^* - \mathbf{r}| > \delta$, and τ is defined as

$$\tau \equiv \frac{\mathbf{e}_x \mathbf{e}_x^* + \mathbf{e}_y \mathbf{e}_y^*}{|\mathbf{r} - \mathbf{r}^*|} \quad (2.3)$$

The inner area integral of F^E can now be reduced directly to its contour integral equivalent:

$$\frac{-F^E}{\mu^2/2} = \int_{\Omega} \oint_{\Omega^*} \mathbf{n}^* \cdot (\nabla \cdot \tau) ds^* d^2\mathbf{r} \quad (2.4)$$

where \mathbf{n}^* is the outward unit normal to Ω^* and s^* is the arc length along the boundary of Ω^* .

Before Green's theorem can be applied to the remaining area integral, eq 2.4 must first be cast into the form of eq 2.1. To do so, two distinct regions of Ω , as shown in Figure 1a, are defined: Ω_1 as all points of Ω located further than δ from the perimeter P , and Ω_2 as all points of Ω located closer than δ to the perimeter. As shown in Figure 1b, when $\mathbf{r} \in \Omega_1$, the boundary of Ω^* consists of two nonintersecting closed loops: P , the perimeter, and C , a circle of radius δ centered at \mathbf{r} . As shown in Figure 1c, when $\mathbf{r} \in \Omega_2$ the boundary of Ω^* is a single closed loop formed by the union of \hat{P} and \hat{C} , where \hat{P} is that portion of P more than δ from \mathbf{r} and \hat{C} is that portion of C which is contained in Ω . The integral in eq 2.4 can thus be expanded as follows:

(11) McConnell, H. M. *Annu. Rev. Phys. Chem.* 1991, 42, 171.

(12) McConnell, H. M.; de Koker, R. *J. Phys. Chem.* 1992, 96, 7101.

(13) Salas, S. L.; Hille, E. *Calculus: One and Several Variables*, 4th ed.; John Wiley and Sons: New York, 1982; Chapter 19.

$$\begin{aligned}
\frac{-F^E}{\mu^2/2} &= [\int_{\Omega_1} \oint_{\Omega^*} + \int_{\Omega_2} \oint_{\Omega^*}] (\mathbf{n}^* \cdot \nabla \cdot \boldsymbol{\tau}) ds^* d^2\mathbf{r} \\
&= [\int_{\Omega_1} \oint_P + \int_{\Omega_1} \oint_C + \int_{\Omega_2} \oint_{(P \cup C)}] (\mathbf{n}^* \cdot \nabla \cdot \boldsymbol{\tau}) ds^* d^2\mathbf{r} \\
&= [\int_{\Omega_1} \oint_P + \int_{\Omega_1} \oint_C + \int_{\Omega_2} \int_P + \int_{\Omega_2} \int_C] (\mathbf{n}^* \cdot \nabla \cdot \boldsymbol{\tau}) ds^* d^2\mathbf{r} \quad (2.5)
\end{aligned}$$

The normal to C , or to \hat{C} , is the unit vector pointing to the center of C . In this case, it can easily be shown that

$$\mathbf{n}^* \cdot \nabla \cdot \boldsymbol{\tau} = -1/\delta^2 \quad (2.6)$$

Hence, the summation of those terms in eq 2.5 which integrate over C or \hat{C} reduces to

$$[\int_{\Omega_1} \oint_C + \int_{\Omega_2} \int_C] (\mathbf{n}^* \cdot \nabla \cdot \boldsymbol{\tau}) ds^* d^2\mathbf{r} = -\frac{2\pi A}{\delta} + \frac{2\pi}{\delta} \int_{\Omega_2} \phi d^2\mathbf{r} \quad (2.7)$$

where A is the area of the domain and $2\pi - \phi$ equals the internal angle of the arc \hat{C} .

The normal to P , or to \hat{P} , is independent of \mathbf{r} . Hence, the summation of those terms in eq 2.5 which integrate over P or \hat{P} may therefore be rewritten as

$$\begin{aligned}
&[\int_{\Omega_1} \oint_P + \int_{\Omega_2} \int_P] (\mathbf{n}^* \cdot \nabla \cdot \boldsymbol{\tau}) ds^* d^2\mathbf{r} = \\
&[\int_{\Omega_1} \oint_P + \int_{\Omega_2} \int_P] \nabla \cdot (\boldsymbol{\tau} \cdot \mathbf{n}^*) ds^* d^2\mathbf{r} \quad (2.8)
\end{aligned}$$

Likewise, the perimeter P of the domain is independent of \mathbf{r} , and therefore

$$\int_{\Omega_1} \oint_P \nabla \cdot (\boldsymbol{\tau} \cdot \mathbf{n}^*) ds^* d^2\mathbf{r} = \int_{\Omega_1} \nabla \cdot \oint_P \boldsymbol{\tau} \cdot \mathbf{n}^* ds^* d^2\mathbf{r} \quad (2.9)$$

Unlike P , however, \hat{P} is a function of \mathbf{r} and from the Leibnitz rule

$$\begin{aligned}
\int_{\Omega_2} \int_P \nabla \cdot (\boldsymbol{\tau} \cdot \mathbf{n}^*) ds^* d^2\mathbf{r} &= \int_{\Omega_2} \nabla \cdot \int_P \boldsymbol{\tau} \cdot \mathbf{n}^* ds^* d^2\mathbf{r} + \\
&\int_{\Omega_2} \left(\nabla \theta_1 \cdot \left(\boldsymbol{\tau} \cdot \mathbf{n}^* \frac{ds^*}{d\theta} \right) \Big|_{\theta_1} - \nabla \theta_2 \cdot \left(\boldsymbol{\tau} \cdot \mathbf{n}^* \frac{ds^*}{d\theta} \right) \Big|_{\theta_2} \right) d^2\mathbf{r} \quad (2.10)
\end{aligned}$$

where θ_1 and θ_2 are the angles at which \hat{P} intersects \hat{C} , as shown in Figure 1b.

Green's theorem can now be applied to the first term on the right-hand sides of eqs 2.9 and 2.10:

$$\begin{aligned}
[\int_{\Omega_1} \nabla \cdot \oint_P + \int_{\Omega_2} \nabla \cdot \int_P] (\boldsymbol{\tau} \cdot \mathbf{n}^*) ds^* d^2\mathbf{r} &= [\oint_{W^+} \oint_P + \oint_{W^-} \int_P + \\
&\oint_P \int_P] \mathbf{n} \cdot \boldsymbol{\tau} \cdot \mathbf{n}^* ds^* ds \quad (2.11)
\end{aligned}$$

where W is the boundary between Ω_1 and Ω_2 , the "+" indicating an outward normal and "-" an inward normal (Figure 1). Since \hat{P} is identical to P when $\mathbf{r} \in W$, the first two terms on the right-hand side of eq 2.11 cancel.

Finally, collecting eqs 2.6, 2.8, and 2.9–2.11, the electrostatic free energy can be written as

$$\begin{aligned}
\frac{F^E}{\mu^2/2} &= \frac{2\pi A}{\delta} - \oint_P \int_P \frac{d\mathbf{X}^* \cdot d\mathbf{X}}{|\mathbf{X} - \mathbf{X}^*|} - \frac{2\pi}{\delta} \int_{\Omega_2} \phi d^2\mathbf{r} - \\
&\int_{\Omega_2} \left(\nabla \theta_1 \cdot \left(\boldsymbol{\tau} \cdot \mathbf{n}^* \frac{ds^*}{d\theta} \right) \Big|_{\theta_1} - \nabla \theta_2 \cdot \left(\boldsymbol{\tau} \cdot \mathbf{n}^* \frac{ds^*}{d\theta} \right) \Big|_{\theta_2} \right) d^2\mathbf{r} \quad (2.12)
\end{aligned}$$

where $\mathbf{X} \in P$ and $\mathbf{X}^* \in \hat{P}$. We shall refer to this expression from here on as the rigorous contour expression (RCE).

B. Reduction from Fourth-Order to Third-Order Integration Using Coordinate Transformation. In the second simplification of the electrostatic energy, the integral is reduced from fourth to third order using a prudent coordinate transformation. Specifically, the inner

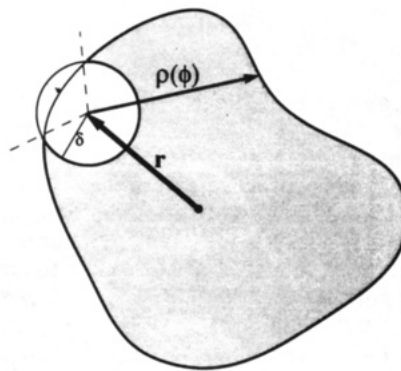


Figure 2. Desired (shaded) region of integration for $\Psi(\mathbf{r})$ which can be selected by applying the Heavyside step function either to ξ or to ϕ , in which case the limits of integration for ϕ are shown with dashed lines.

area integral of eq 1.3, defined here as $\Psi(\mathbf{r})$, is rewritten using polar coordinates with origin at \mathbf{r} :

$$\begin{aligned}
\Psi(\mathbf{r}) &= \int \mathcal{H}(|\mathbf{r}^* - \mathbf{r}| - \delta) |\mathbf{r}^* - \mathbf{r}|^{-3} d^2\mathbf{r}^* = \\
&\int_0^{2\pi} \int_0^{\rho(\phi)} \frac{\mathcal{H}(\xi - \delta)}{\xi^3} \xi d\xi d\phi \quad (2.13)
\end{aligned}$$

Here $\xi = |\mathbf{r}^* - \mathbf{r}|$ and $\rho(\phi)$ is the distance from \mathbf{r} to the domain boundary at polar angle ϕ . Alternatively, the same region of integration can be achieved by raising the lower limit on ξ to δ and restricting ϕ to those angles for which $\rho(\phi) > \delta$, as illustrated in Figure 2. In this case, $\Psi(\mathbf{r})$ takes the form

$$\Psi(\mathbf{r}) = \int_0^{2\pi} \mathcal{H}(\rho(\phi) - \delta) \int_{\delta}^{\rho(\phi)} \frac{1}{\xi^3} \xi d\xi d\phi \quad (2.14)$$

The integral over ξ can now be evaluated analytically:

$$\Psi(\mathbf{r}) = \int_0^{2\pi} \mathcal{H}(\rho(\phi) - \delta) \left(\frac{1}{\delta} - \frac{1}{\rho(\phi)} \right) d\phi \quad (2.15)$$

Using the relationship $\mathcal{H}(x) = 1 - \mathcal{H}(-x)$, $\Psi(\mathbf{r})$ can be rewritten as

$$\begin{aligned}
\Psi(\mathbf{r}) &= \frac{2\pi}{\delta} - \int_0^{2\pi} \frac{1}{\rho(\phi)} \mathcal{H}(\rho(\phi) - \delta) d\phi - \\
&\int_0^{2\pi} \frac{1}{\delta} \mathcal{H}(\delta - \rho(\phi)) d\phi \quad (2.16)
\end{aligned}$$

or more simply

$$\Psi(\mathbf{r}) = \frac{2\pi}{\delta} - \int_0^{2\pi} \frac{1}{\rho^*(\phi)} d\phi \quad (2.17)$$

where $\rho^*(\phi)$ is defined to be the greater of $\rho(\phi)$ and δ . Substituting eq 2.17 in eq 1.3, the electrostatic free energy can be written as

$$\frac{F^E}{\mu^2/2} = \frac{2\pi A}{\delta} - \int_0^{2\pi} \int_0^{2\pi} \frac{1}{\rho^*(\phi)} d\phi d^2\mathbf{r} \quad (2.18)$$

We shall refer to this expression from here on as the coordinate transformation expression (CTE).

3. Numerical Evaluation of the Electrostatic Energy

All of the values of F^E reported in this paper were computed numerically using trapezoid rule integration. All area integrals were evaluated in polar coordinates. The discretization of each integral, however, depended upon the form of its integrand.

Integrals in which the integrand was of similar magnitude for the entire range of integration were discretized

uniformly; i.e.

$$\Delta x_i = \alpha_x \quad (3.1)$$

Here x is some variable of integration and α_x is the distance between the nodes in x . To ensure convergence of integration, each α was repeatedly halved until the relative difference between consecutive values of the integral was less than 0.01%. This discretization method was used to evaluate the integrals over the angular component of \mathbf{X} in the RCE and the capacitor approximation, the radial and angular components of \mathbf{r} in the RCE, and the angular component of \mathbf{r} in the CTE.

Integrals in which the integrand varied by many orders of magnitude over the range of integration were discretized nonuniformly such that the distance between nodes was inversely proportional to the integrand; i.e.

$$\Delta x_i = \frac{\beta_x}{\text{integrand}(x_i)} \quad (3.2)$$

Here x is again some variable of integration and β_x is a proportionality constant for the distance between the nodes in x . As with the α 's, each β was repeatedly halved until consecutive values of the integral differed by less than 0.01%. This discretization method was used for the integrals over the angular component of \mathbf{X}^* in the RCE and the capacitor approximation, ϕ in the CTE, and the radial component of \mathbf{r} in the CTE.

4. Comparison of the Computational Efficiency of the RCE and the CTE

Both the rigorous contour expression (eq 2.12) and the coordinate transformation expression (eq 2.18) can be computed more efficiently than the original formulation of the electrostatic energy (eq 1.3). Because the RCE requires only second-order integration while the CTE requires third-order integration, it would appear that the RCE can always be calculated more efficiently than the CTE. The RCE, however, contains the integral over the terms which include $\nabla\theta_1$ and $\nabla\theta_2$. The relationship between θ_1 (or θ_2) or \mathbf{r} is defined implicitly through the law of cosines (see Figure 1b); i.e.

$$r^2 + R^2(\theta_1) - 2rR(\theta_1) \cos(\theta_1 - \theta) - \delta^2 = 0 \quad (4.1)$$

where r and θ are the polar components of \mathbf{r} and $R(\theta_1)$ is the magnitude of \mathbf{X} at angle θ_1 . Newton's method or some other iterative root locating algorithm must be used to determine θ_1 for each r . Therefore, $\nabla\theta_1$ (or $\nabla\theta_2$) must be evaluated numerically with a technique such as forward differencing:

$$\nabla\theta_1 \approx \frac{\theta_1|_{(r+\Delta r, \theta)} - \theta_1|_{(r, \theta)}}{\Delta r} \mathbf{e}_r + \frac{\theta_1|_{(r, \theta+\Delta\theta)} - \theta_1|_{(r, \theta)}}{\Delta\theta} \mathbf{e}_\theta \quad (4.2)$$

where Δr and $\Delta\theta$ are small but finite perturbations. Because of the extra iterative calculations required to evaluate $\nabla\theta_1$ and $\nabla\theta_2$, the RCE cannot be computed as efficiently as the CTE.

The RCE can recover its numerical efficiency, however, if the $\nabla\theta$'s are approximated by assuming that the curvature of the domain boundary is insignificant (as detailed in the Appendix). While this approximation is accurate for large circular domains ($R \gg \delta$), it becomes increasingly inaccurate as the domain becomes less circular. This is demonstrated in Figure 3 which shows the difference between the approximated RCE and the CTE for regularly undulating domains of the form $R(\theta) = \mathcal{R}(1 - \epsilon \cos(m\theta))$. In brief, the RCE can be calculated more efficiently than the CTE for domains which are nearly

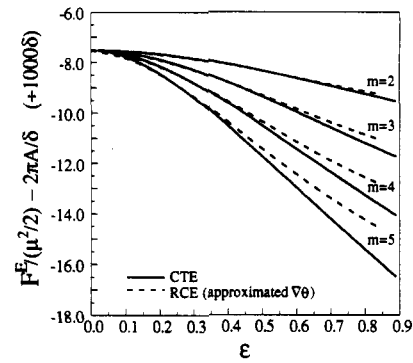


Figure 3. Electrostatic energy as determined by both the CTE and the approximated RCE for four series of domain shapes, defined by $R(\theta) = \mathcal{R}(1 - \epsilon \cos(m\theta))$. \mathcal{R} was chosen such that the domain area equals that of a circle with radius 100 δ .

circular because $\nabla\theta_1$ and $\nabla\theta_2$ can be approximated accurately. Otherwise the CTE should be used.

5. Comparison of Domain Morphology Results Based on the Rigorous Expressions and the Capacitor Approximation

The free energy theory of McConnell (eq 1.1) can be used to predict domain shapes and associated shape transitions. Previous applications of this theory, however, have been based primarily on the capacitor approximation to the electrostatic energy. Using our simplified, yet rigorously derived, expressions of the electrostatic energy, we have repeated two of these domain morphology calculations: the equilibrium radius of circular domains and the transition from circular to elliptical domain shapes.

The equilibrium radius, R_{eq} , of circular domains in a film with a fixed area fraction of domains, ϕ , can be determined using the method described by McConnell and Moy.⁹ The number of domains per unit area in such a film is $\phi/(\pi R_{eq}^2)$, and the resulting free energy is

$$F = \frac{\phi}{\pi R^2} (F^I + F^E) \quad (5.1)$$

where F^I and F^E are the interfacial and electrostatic energies per domain of radius R . For a given ratio of λ to μ^2 , the equilibrium radius is that value of R which minimizes F . Using the capacitor approximation, McConnell and Moy⁹ determined analytically that the equilibrium radius is $(e^3\delta/4)e^{\lambda/\mu^2} (\approx 5.02\delta e^{\lambda/\mu^2})$. Using the RCE, we calculated F as a function of R , and determined R_{eq} for various λ/μ^2 . Our results could be fit accurately with the curve $R_{eq} = 0.67\delta e^{1.0\lambda/\mu^2}$ (correlation coefficient 0.9998).

A transition from a circular domain to an elliptical domain is predicted when λ/μ^2 is greater than some critical value; above this value, the free energy of an elliptical domain is lower than that of a circular one. The onset of this transition can be determined through an analysis of the variation of free energy with elliptical eccentricity, b/a , where b and a are the lengths of the principle axes. A plot of free energy versus eccentricity has zero slope at $b/a = 1$, i.e., circular domains, because ellipses with eccentricity a/b are 90° rotations of ellipses with eccentricity b/a . Therefore, the transition from circular to elliptical domains occurs when the second derivative of free energy evaluated at $b/a = 1$ equals zero. Using the capacitor approximation, Keller et al.⁸ determined analytically that this shape transition occurs when $\lambda/\mu^2 = -10/3 + \ln(4R/\delta)$ where R is the radius of the circular domain. Using the RCE, we calculated the critical value of λ/μ^2 with the following algorithm. From a plot of F versus b/a for a given domain area, we determined

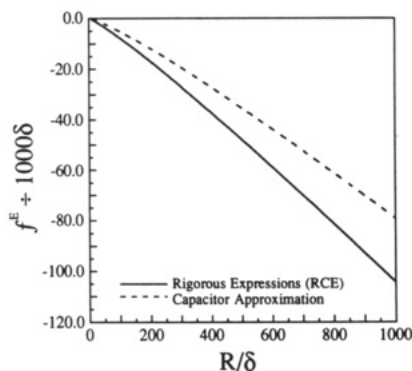


Figure 4. Capacitor approximation and the RCE values of f^E for circular domains as a function of domain radius.

numerically the second derivative at $b/a = 1$ for various λ/μ^2 . Then from a plot of these results, we determined the value of λ/μ^2 for which this second derivative was zero. Repeating this procedure for various domain areas, we found that the onset of the shape transition could be fit accurately with the curve $\lambda/\mu^2 = -1.33 + 1.0 \ln(4R/\delta)$ (correlation coefficient 1.0000).

Clearly the capacitor approximation and the RCE produce significantly different results. The source of the difference between these two functionals can be identified readily by comparing the capacitor approximation (eq 1.5) with the RCE (eq 2.12). Although the term which is proportional to area differs between the two expressions, this difference does not affect results of domain morphology calculations in which the area is held constant, such as those described above. Therefore, as a basis for comparison, it is convenient to define a new variable f^E through the relationship

$$\frac{-F^E}{\mu^2/2} \equiv \chi A + f^E \quad (5.2)$$

where $\chi = 4\pi/t$ for the capacitor approximation and $\chi = 2\pi/\delta$ for the RCE (or the CTE). Furthermore, we define Δf^E to be the difference between f^E for the RCE and the capacitor approximation:

$$\Delta f^E = -\frac{2\pi}{\delta} \int_{\Omega_2} \phi \, d^2\mathbf{r} - \int_{\Omega_2} \nabla\theta_1 \cdot \left(\boldsymbol{\tau} \cdot \mathbf{n}^* \frac{ds^*}{d\theta} \right) \Big|_{\theta_1} - \int_{\Omega_2} \nabla\theta_2 \cdot \left(\boldsymbol{\tau} \cdot \mathbf{n}^* \frac{ds^*}{d\theta} \right) \Big|_{\theta_2} \, d^2\mathbf{r} \quad (5.3)$$

It is this difference which affects the results of constant area morphology calculations.

Both of the domain morphology calculations described above were based on the free energy of circular domains. Figure 4 shows as a function of radius two plots of f^E for a circular domain: one determined using the capacitor approximation, the other using the RCE. The difference between these two curves is proportional to the domain perimeter, $\Delta f^E = -4.0P$. Hence, from eq 5.2, the capacitor approximation overestimates F^E by $2.0\mu^2P$. This has the same affect on the total free energy as overestimating the line tension by $2.0\mu^2$. Consequently, for this special case of circular domains, free energy calculations based on the capacitor approximation can be made to match those based on the RCE simply by replacing the line tension used in the capacitor approximation with an artificial line tension equal to $\lambda - 2.0\mu^2$. This can be easily verified in the two preceding examples. Moreover, because the capacitor approximation has been shown to match \bar{F} when the line tension used in the capacitor approximation is replaced with $\lambda - \mu^2$, a bridge can be forged between the two energy

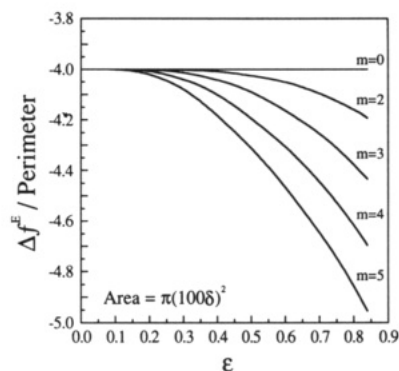


Figure 5. Difference in f^E between the capacitor approximation and the rigorous expressions for undulating domains as defined in the text. The domain area equals that of a circle with radius 100δ .

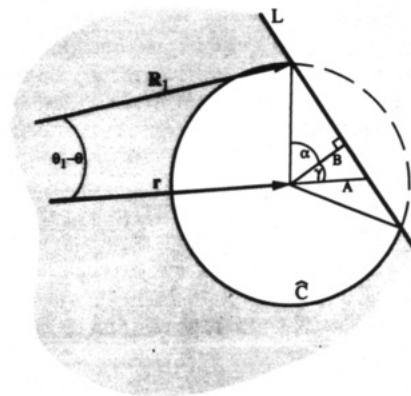


Figure 6. Geometric definitions used to approximate $\nabla\theta_1$. The perimeter of the domain is represented with the straight line L . The remaining vectors, line segments, and angles are defined in the Appendix. The origin is located to the far left of the figure.

functionals F and \bar{F} . Specifically, for the case of circular domains, \bar{F} can be made to equal F simply by adjusting the line tension, $\lambda_{\bar{F}} = \lambda_F - \mu^2$, or equivalently by adjusting the nearest-neighbor parameter, $\delta_{\bar{F}} = \delta_F/e$.

The capacitor approximation has also been used to determine free energy of noncircular domains. Vanderlick and Möhwald,¹⁰ for example, used it to predict the shape transitions of domains with regularly undulating boundaries. Figure 5 shows $\Delta f^E/P$ for this class of domain shapes, given by $R(\theta) = R(1 - \epsilon \cos(m\theta))$. Clearly Δf^E is not proportional to the perimeter for noncircular domains. Consequently, shape calculations based on noncircular domains depend strongly on the choice of energy functional and cannot be coerced into agreement simply by adjusting the line tension. Rather than repeating Vanderlick and Möhwald's calculation, which is restricted to a particular class of domain shapes, we are currently using functional minimization to solve directly for the exact domain shape which minimizes the free energy.¹⁴

Acknowledgment. We gratefully acknowledge the support of the donors of the Petroleum Research Fund, administered by the American Chemical Society, and the support of the National Science Foundation, through a Presidential Young Investigator Award (CTS-89-57051) to T.K.V. and a National Science Foundation Fellowship to M.A.M. We also thank Harden McConnell for providing us with preprints of his work.

(14) Mayer, M. A.; Vanderlick, T. K. To be submitted for publication to *SIAM J. Appl. Math.*

Appendix

The integrand of the final term of the RCE contains the two divergences $\nabla\theta_1$ and $\nabla\theta_2$. Using polar coordinates, these gradients may be expressed as

$$\begin{aligned}\nabla\theta_1 &= \frac{\partial\theta_1}{\partial r} \mathbf{e}_r + \frac{1}{r} \frac{\partial\theta_1}{\partial\theta} \mathbf{e}_\theta \\ \nabla\theta_2 &= \frac{\partial\theta_2}{\partial r} \mathbf{e}_r + \frac{1}{r} \frac{\partial\theta_2}{\partial\theta} \mathbf{e}_\theta\end{aligned}\quad (\text{A.1})$$

The derivatives above may either be solved iteratively or approximated by assuming that the curvature of the domain boundary is negligible on the scale of the δ . In such a situation, the geometry of the system about θ_1 may be defined as shown in Figure 6. Let $\mathbf{r} = (r, \theta)$ be the point at which we want to know $\nabla\theta_1$ and $\nabla\theta_2$, \mathbf{R}_1 the vector to the perimeter at θ_1 , R_1 the magnitude of $\mathbf{R}(\theta_1)$, L the line approximating the perimeter, A the distance from \mathbf{r} to L , colinear with \mathbf{r} , B the distance from \mathbf{r} to L , perpendicular to L , γ the angle between line segments A and B , and α the angle between line segment B and $\mathbf{R}_1 - \mathbf{r}$. It follows then from the geometry of the problem that

$$\begin{aligned}\gamma &= \sin^{-1} \left(\frac{R'(\theta)}{(R^2(\theta) + R'^2(\theta))^{1/2}} \right) \quad A = R(\theta) - r \\ B &= A \cos \gamma \quad \alpha = \cos^{-1}(B/\delta) \\ R_1 &= (\delta^2 + r^2 + 2r\delta \cos(\alpha + \gamma))^{1/2} \\ \theta_1 &= \theta + \sin^{-1} \left(\frac{\sin(\alpha + \gamma)}{R_1/\delta} \right)\end{aligned}\quad (\text{A.2})$$

Differentiation of θ_1 yields

$$\frac{\partial\theta_1}{\partial r} = \frac{\delta/R_1}{\cos(\theta_1 - \theta)} \left[\frac{\cos(\alpha + \gamma) + (r\delta/R_1^2) \sin^2(\alpha + \gamma)}{(\delta^2 - B^2)^{1/2}} \cos \gamma - \frac{r + \delta \cos(\alpha + \gamma)}{R_1^2} \sin(\alpha + \gamma) \right] \quad (\text{A.3a})$$

and

$$\frac{\partial\theta_1}{\partial\theta} = 1 + \frac{\delta/R_1}{\cos(\theta_1 - \theta)} \left[\left(\cos(\alpha + \gamma) + \frac{r\delta}{R_1^2} \sin^2(\alpha + \gamma) \right) \times \left(\frac{A\gamma' \sin \gamma - R'(\theta) \cos \gamma}{(\delta^2 - B^2)^{1/2}} + \gamma' \right) \right] \quad (\text{A.3b})$$

where $\gamma' = \partial\gamma/\partial\theta = (R'^2(\theta) - R(\theta)R''(\theta))/(R^2(\theta) + R'^2(\theta))$. Similarly, differentiation of θ_2 yields

$$\frac{\partial\theta_2}{\partial r} = \frac{-\delta/R_2}{\cos(\theta - \theta_2)} \left[\frac{\cos(\alpha - \gamma) + (r\delta/R_2^2) \sin^2(\alpha - \gamma)}{(\delta^2 - B^2)^{1/2}} \cos \gamma - \frac{r + \delta \cos(\alpha - \gamma)}{R_2^2} \sin(\alpha - \gamma) \right] \quad (\text{A.4a})$$

and

$$\frac{\partial\theta_2}{\partial\theta} = 1 - \frac{\delta/R_2}{\cos(\theta - \theta_2)} \left[\left(\cos(\alpha - \gamma) + \frac{r\delta}{R_2^2} \sin^2(\alpha - \gamma) \right) \times \left(\frac{A\gamma' \sin \gamma - R'(\theta) \cos \gamma}{(\delta^2 - B^2)^{1/2}} - \gamma' \right) \right] \quad (\text{A.4b})$$